EUROPEAN LABORATORY FOR PARTICLE PHYSICS

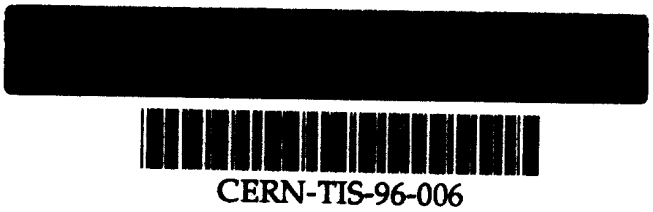

CERN/TIS-RP/96-06

CERN-TIS-96-006

RADIOLOGICAL IMPLICATIONS OF THE RELEASE OF AIR FROM THE LHC EXPERIMENTAL REGIONS

M. Huhtinen, L. E. Moritz, K. M. Potter,
S. Rollet and G. R. Stevenson

Abstract

The present report contains an estimation of the release of radioactivity in the air produced in the ATLAS and CMS experiments. The latest version of the FLUKA code was used to simulate the hadronic cascades initiated by the primary p-p events; the latter had previously been created with the DTUJET93 event generator which included single diffraction. 39 different radionuclides are considered. Their production was estimated from the hadron track-lengths in the air volumes of the experimental caverns using a newly-developed cross-section set. The release of the radionuclides from the caverns has been estimated using a model which assumes the complete mixing of the air inside the detectors and the caverns. The effect of these releases has been evaluated by determining the off-site doses and dose rates due to the radioactive emissions calculated using the procedures described by the Swiss HSK. The pathways of exposure in the CERN environment which are considered here include the external dose from the radioactive plume, exposure to radionuclides deposited on the ground, the internal dose from the inhalation of radioactive air, the ingestion of vegetables grown in affected areas and the ingestion of meat and dairy products from livestock which graze in the affected area.

The estimated annual dose due to the release of air from the experimental caverns never exceeds the equivalent of 25 minutes of exposure to natural background radiation.

CERN, Geneva, Switzerland
1 April 1996

1. Introduction

This report is an update of the estimation of radioactivity in the air of the LHC experimental caverns reported in [Ste92]. In the present work, however, the geometrical form of the detectors inside the caverns have been described in a much more complete manner and the ATLAS and CMS experiments are considered individually.

Whereas only 18 radionuclides were considered in the original study, 39 different radionuclides are considered here. Their production was estimated from the hadron track-lengths in the air using a newly-developed cross-section set. The release of the radionuclides from the caverns has been estimated in a similar manner to that of [Ste92] but now the effect of these releases has been evaluated by determining the off-site doses and dose rates due to the radioactive emissions. These have been calculated using the procedures described in a draft of a document issued by the Swiss HSK (Hauptabteilung für die Sicherheit der Kernanlagen) [HSK95]. Wherever this document is incomplete, the IAEA Safety Guide [IAEA80] has been used to complete or clarify the procedure. The details of this model are described in a separate report [Mor96]. The pathways of exposure in the CERN environment which are considered here include the external dose from the radioactive plume, exposure to radionuclides deposited on the ground, the internal dose from the inhalation of radioactive air, the ingestion of vegetables grown in affected areas and the ingestion of meat and dairy products from livestock which graze in the affected area. Because the dose calculations require several individual steps each of which incorporates a measure of conservatism that is then applied sequentially, the dose rates calculated in this way are expected to be conservative.

2. Simulations for the ATLAS Experimental Region

Description of the Geometry

The geometry of the ATLAS experimental region implemented in FLUKA for these calculations was identical to that developed for the Technical Proposal as described in [Fer96] and is shown in Figures 1 and 2. In this description the complex geometry of the detector, the experimental hall and the two vertical shafts has been simulated with great care. In addition the description contains a correct assignment of material composition to the different regions for all the sub-detectors, cables ducts and gaps between them, all of which which could be important for streaming.

Such a detailed description however leads to a large number of different air regions, which, for the purpose of this work, were combined to give the production in only seven main regions:

- The "inner tracker" region is obtained by summing all the air regions surrounding the Transition Radiation (TRT) and the Semi-Conductor Tracker described in the central cavity.
- All the air regions present around the Ecal and Hcal, including the gaps at the end of the barrel and the extended barrel tile calorimeters, are summed together to define the second region.
- The third (FW-cones) is a small region in front and inside the forward integrated LAr calorimeters.
- The fourth (VFcal-collimator) is the very forward part, inside the inner bore of the end cap toroid, in front and around the collimator for the low-beta quadrupole.

- The fifth (cavern) includes all the air in the experimental hall and the air surrounding the barrel and forward muon chambers and the collimator shielding.
- The last two regions are the large and small shafts.

The volume of these combined regions is given in Table 1. The number of regions existing in the real situation is also given.

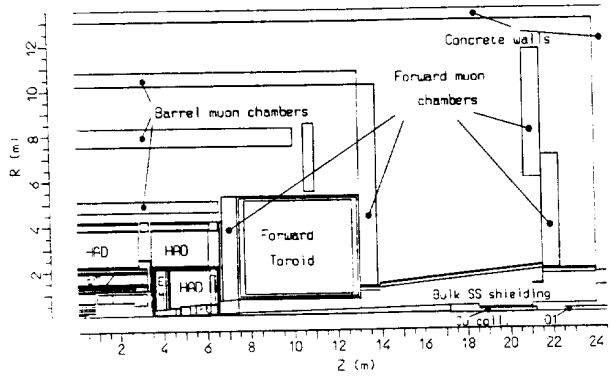

Figure 1: The ATLAS detector geometry used in FLUKA

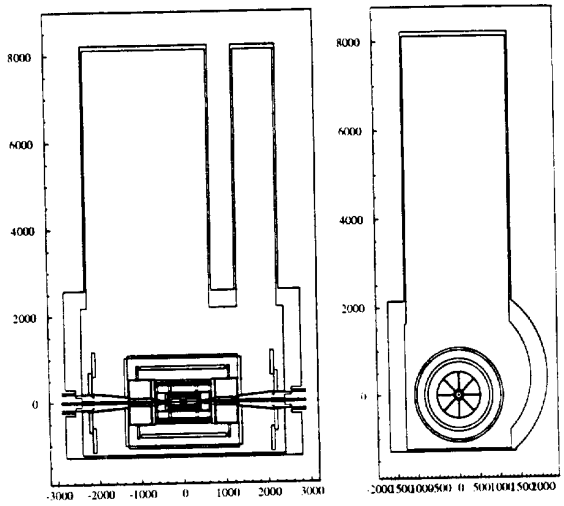

Figure 2: The geometry of the ATLAS cavern and shafts used in the FLUKA simulations. Cut through the zy plane (left) and through the xy plane (right).

Table 1: Air regions inside and around the ATLAS and CMS detectors.

Index	Region	Number	ATLAS Volume (m^3)	CMS Volume (m^3)
1	Inner Tracker	1	11.9	33.9
2	ECAL-HCAL	1	109.0	26.5
3	FW-cones	2	0.034	12.2
4	VFCAL-Collimator	2	5.4	2.76
5	Cavern	1	37800	23800
6	Large Shaft	1	35700	21100
7	Small Shaft	1	6120	

Simulations

The latest version of the FLUKA code [Fas93, Fas94] was used to simulate the hadronic cascades initiated by the primary p-p events and to determine the track-lengths of protons, charged pions and neutrons as a function of energy in the different regions containing air in the caverns. The primary p-p events were created previously with the DTUJET93 [Aur94] event generator which included single diffraction. The DTUJET secondaries file used in these simulations was created from 1300 primary p-p events, including diffractive events, which gave an average multiplicity of 120

secondaries per event. At the beginning of the calculations and at the end of each event, a new p-p collision was randomly selected from the file and its secondaries banked in the simulation stack.

Seven runs were made of 100 primary events each, *i.e.* around 84000 secondaries were considered for these calculations.

3. Simulations for the CMS Experimental Region

Description of the Geometry

The geometrical description of the experiment and the cavern was adapted from the "standard" description used for the CMS radiation-studies [Huh95a]. The large number of different air volumes was reduced in the present simulations by judicious combination. For example, the exact description of the tracker was removed, as were all muon chambers except for the last forward one (MF4). The hadronic and forward calorimeters and the iron yoke were modelled as solid iron blocks. For simplicity, only one side ($z > 0$) of the CMS detector and low-β regions were modelled in detail, see Figure 3.

Previous simulations indicated that the leakage of radiation from one forward part of the cavern to the other is negligible, since the detector forms an almost hermetic plug in the centre of the cavern [Huh95b]. Nevertheless the air-region around the detector was extended to the back wall of the cavern, see Figure 3. Fluxes in the inner detector at negative z are also not negligible; thus the interior was fully described on both sides of the interaction point up to the very forward calorimeter (VFCAL).

The main shaft was placed on the forward side of the geometry and the description of the inner triplet area up to D2 was taken from [Huh95c].

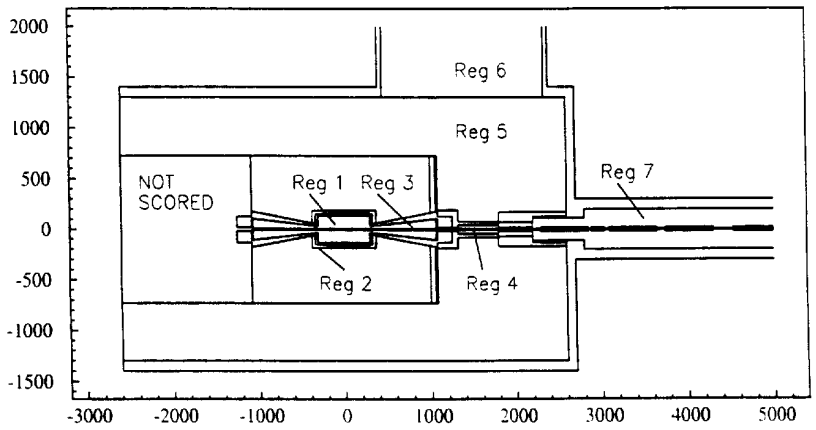

Figure 3: Geometry used for the asessment of track-length in air inside and around the CMS experiment.

The air volumes in the CMS experimental region were also separated into seven conceptually different regions, listed in Table 1. The central tracking cavity was treated as a single unit: it will most probably have its own ventilation system, separated from that of the hall. The gap between the electromagnetic (ECAL) and hadronic (HCAL) calorimeters is not yet well defined, but will include at least some air. This region should not be very important but has been separated from the

others in this study. The forward cones, from the tracker up to the VFCAL, are intermediate volumes for which the ventilation system has not yet been defined. They could finally be connected to the volume inside and behind the VFCAL, but for these calculations they are kept separate. The largest volume is that outside the CMS detector, *i.e.* all the air in the cavern which is not enclosed in the forward shielding or the detector itself. The ventilation system of the main shaft will probably be separate from that of the cavern, and therefore this shaft naturally forms a separate volume. The seventh volume is the tunnel containing the low-beta quadrupoles extending up to the recombination dipole D2. This region has not been included in the present analysis and will be the object of a future study.

The volumes of the different regions are also listed in Table 1.

Simulation

As for the ATLAS simulations, primary events were generated with the DTUJET93 [Aur94] event generator which includes diffractive scattering. However the position of the secondaries in the file was randomized so that sequential interrogation of the file could take place from any starting point and always yield secondaries from "average" events. Secondaries were transported with the FLUKA95 code [Fas93, Fas94].

The simulation method was adopted from [Huh95c], *i.e.* the source was divided into very-forward ($\theta > 732\mu$rad) and "central" contributions. Eight runs, each treating 5000 "central" tracks and another eight treating 500 forward tracks were performed. For the experimental cavern, only the contribution from the central tracks was considered.

4. Determination of track-lengths

For both the ATLAS and CMS simulations, track-length was scored on a region basis using a logarithmic energy binning with ten bins per decade. The lower limit for charged hadrons was 10 MeV and the upper limit 10 TeV. Low-energy neutrons were scored in the 72-group structure of FLUKA. For neutrons the upper energy limit was 10 TeV. Since the upper bound of the low-energy neutron group structure is 19.6 MeV, 57 logarithmic bins will have a factor width of 1.2593, which is close to $10^{0.1} = 1.2589$. By default FLUKA normalizes track-lengths by assuming that all regions have a volume of 1 cm^3. The total track-length in the regions is thus obtained directly. Integrated track-lengths for the two experimental regions are given in Table 2, separated according to hadron type and energy.

ATLAS – CMS comparison

The p-p events are identical for the two high-luminosity experiments, but the experiments themselves are quite different, so that the integrated track-lengths and resulting radionuclide production rates can be substantially different.

Table 1, which shows the volumes of the regions, best illustrates the differences between the experiments.

Table 2: Integrated track-length in cm/event in the different regions of the experimental areas. The Total 'Hall" shows the sum over regions 1–5.

Index	Region	p	$\pi^{\pm}$	n ($E > 19.6$ MeV)	n (th< $E < 19.6$ MeV)	n (thermal)
ATLAS						
1	Inner Tracker	880	12000	2000	40000	27000
2	ECAL-HCAL	30	160	330	20000	3100
3	FW-cones	160	1000	450	14000	230
4	VFCAL-Collimator	2700	17000	13000	640000	0
5	Hall	40	120	2200	49000	18000
6	Large Shaft	6	1	370	9300	6800
7	Small Shaft	1	0.01	90	480	530
	Total "Hall"	3800	30000	18000	760000	48000
CMS						
1	Inner Tracker	2000	15000	4400	34000	55000
2	ECAL-HCAL	120	330	1600	105000	10
3	FW-cones	5200	30000	10500	155000	25000
4	VFCAL-Collimator	2900	15500	9100	310000	1300
5	Hall	980	670	32000	105000	33000
6	Large Shaft	120	20	5200	28000	14500
	Total "Hall"	11000	62000	58000	710000	92000

The tracker volume in ATLAS is roughly one third of that of the CMS tracker, since most of the space is taken by the TRT of ATLAS. The free space, however, is at small radii, where the charged track density is highest. Therefore the difference in high-energy track-lengths is smaller than the ratio of volumes. The low-energy and thermal neutrons are generated mainly in the ECAL and so are influenced by the ECAL material itself (Pb/LAr in ATLAS and $PbWO_4$ in CMS). Also the moderator configurations are significantly different, so that the two experiments really have their own characteristics as far as the neutron flux in the tracker cavity is concerned.

The volumes between the ECAL and the HCAL are very different for the two experiments. In addition they are not well defined for either of the two. The available space will be essentially filled with electronics and cables, which are not included in the simulations. Thus not only a comparison is unjustified, the numbers themselves should be taken to be very tentative and pessimistic, since the volumes of the air-filled regions are certainly overestimated.

Due to the integrated VFCAL the forward cones of ATLAS have shrunk essentially to zero size, whereas they contribute almost half of the high-energy track-length in CMS – and thus are likely to give about half of the total radionuclide production.

The region between the VFCAL and the collimator, but inside the shielding, is larger in ATLAS – including, what in CMS is in the forward cones. But in ATLAS this region is in the shadow of the VFCAL and thus has a decreased contribution from high-energy tracks. As expected, the volume ratio of two is reflected in the low energy neutron fluxes. The origin of zero thermal flux in ATLAS is not yet understood.

The hall of ATLAS is about 50% larger than that of CMS. Due to the thinner shielding around the collimators, the fluxes in the CMS hall are significantly higher and in the low-energy and thermal

neutron fluxes a difference of a factor of 2 can be observed. In the high-energy part of the particle spectrum, the fluxes in CMS are about 10 times higher than in ATLAS. This factor of 10 is in good agreement with the difference in the effectiveness of the shielding around the collimator region. The smaller difference in the low-energy neutron flux is due to the fact that the cascades, which in ATLAS are mainly contained in the shield, develop in the walls of the CMS cavern. So the total number of neutrons produced is not very different and the neutron containment in the ATLAS shield is not much better than in the CMS cavern walls.

The same arguments can be applied to the large shafts as for the hall.

As far as production rates are concerned, the above discussion of Table 2 means that typical high-energy activation products, *i.e.* most of the isotopes, should be produced in CMS at rates of up to 10 times higher than in ATLAS. This difference arises from both the different shielding around the collimator and the supression of high-energy tracklength due to the integrated VFCAL of ATLAS. However the quantity of typical products from neutron activation – ^{14}C and ^{41}Ar in particular – in the two experiments should not differ by more than a factor of two.

5. Determination of the radionuclide production

The 39 radionuclides of interest in this study are listed in Table 3 together with their half-lives taken from [ICRP83]. The track-lengths determined using the FLUKA simulations were multiplied by energy-dependent cross-sections for the production of these radionuclides. These cross-sections were determined by considering the systematics of results from dedicated simulations using the event generators of FLUKA together with data from the compilation of cross-sections by Iljinov *et al.* [Ilj93] and the Silberberg-Tsao parametrizations [Sil90]. Partial cross-sections for radionuclide production by low-energy neutrons were taken from the cross-section files used in FLUKA.

Details of the radionuclide production per p-p collision in each of the air-volumes determined from the ATLAS and CMS simulations are given in Appendix A. The upper bound for the environmental effects due to the release of these radionuclides will be given by the ventilation scenario which results in their release after the shortest delay. The highest production rate is in the inner volumes which must mix with air from the outer volumes before reaching the release point. In these circumstances the upper bound is given by the assumption of total mixing of all the volumes of the main cavern. It is in fact more probable that the air around the inner detectors and inside the forward shielding will mix only slowly or not at all with the outer less activated volumes.

The vertical shafts leading to the experimental caverns are so large that it would be uneconomical and totally unnecessary to ventilate them during machine operation, hence they will be closed at their upper and lower extremities. Any release from these volumes will only occur when they are opened at the start of a shutdown to allow access.

Thus in Table 3 the production for regions 1–5 has been summed to be consistent with the assumption of total mixing, while the values for the production in the various vertical shafts are shown separately.

Table 3: Production of radionuclides in the air of the experimental caverns (in nuclei per p-p collision)

Radionuclide	Half-life	ATLAS			CMS	
		Cavern	Large Shaft	Small Shaft	Cavern	Large Shaft
^{3}H	12.35 y	5.01×10^{-2}	2.02×10^{-4}	4.11×10^{-5}	1.11×10^{-1}	1.59×10^{-3}
^{7}Be	53.3 d	1.50×10^{-2}	4.00×10^{-5}	9.77×10^{-6}	3.54×10^{-2}	2.96×10^{-4}
^{10}Be	1.6×10^{6} y	8.53×10^{-3}	1.22×10^{-4}	2.38×10^{-5}	2.59×10^{-2}	9.81×10^{-4}
^{11}C	20.38 m	2.35×10^{-2}	8.49×10^{-5}	1.98×10^{-5}	6.35×10^{-2}	6.47×10^{-4}
^{14}C	5730.0 y	3.65×10^{0}	4.14×10^{-1}	3.19×10^{-2}	7.82×10^{0}	4.70×10^{-1}
^{13}N	9.965 m	2.33×10^{-2}	2.21×10^{-4}	4.65×10^{-5}	6.74×10^{-2}	1.71×10^{-3}
^{14}O	71.0 s	1.25×10^{-3}	4.36×10^{-6}	1.02×10^{-6}	3.69×10^{-3}	3.53×10^{-5}
^{15}O	122.2 s	1.61×10^{-2}	9.94×10^{-5}	2.28×10^{-5}	4.65×10^{-2}	7.32×10^{-4}
^{19}O	27.1 s	2.91×10^{-6}	2.08×10^{-10}	3.17×10^{-11}	5.53×10^{-6}	1.70×10^{-9}
^{18}F	109.8 m	4.91×10^{-5}	1.79×10^{-8}	2.21×10^{-9}	9.98×10^{-5}	1.30×10^{-7}
^{23}Ne	28.0 s	6.12×10^{-6}	1.34×10^{-9}	2.13×10^{-10}	1.21×10^{-5}	9.53×10^{-9}
^{24}Ne	3.38 m	1.45×10^{-6}	1.57×10^{-10}	2.45×10^{-11}	2.80×10^{-6}	1.19×10^{-9}
^{22}Na	2.602 y	1.76×10^{-5}	1.31×10^{-8}	2.40×10^{-9}	3.66×10^{-5}	8.06×10^{-8}
^{24}Na	15.0 h	2.29×10^{-5}	2.23×10^{-8}	4.72×10^{-9}	4.91×10^{-5}	1.40×10^{-7}
^{25}Na	60.0 s	9.97×10^{-6}	3.97×10^{-9}	6.62×10^{-10}	2.02×10^{-5}	2.67×10^{-8}
^{27}Mg	9.5 m	9.88×10^{-6}	9.90×10^{-9}	1.76×10^{-9}	2.17×10^{-5}	6.34×10^{-8}
^{28}Mg	20.91 h	3.55×10^{-6}	7.71×10^{-9}	1.66×10^{-9}	8.31×10^{-6}	4.84×10^{-8}
^{26}Al	7.16×10^{5} y	2.57×10^{-5}	1.39×10^{-8}	2.44×10^{-9}	5.42×10^{-5}	9.13×10^{-8}
^{28}Al	2.24 m	6.17×10^{-5}	6.54×10^{-8}	1.28×10^{-8}	1.39×10^{-4}	4.11×10^{-7}
^{29}Al	6.6 m	1.88×10^{-5}	3.15×10^{-8}	6.14×10^{-9}	4.37×10^{-5}	1.96×10^{-7}
^{31}Si	157.3 m	3.63×10^{-5}	5.27×10^{-8}	1.24×10^{-8}	8.50×10^{-5}	3.38×10^{-7}
^{32}Si	450.0 y	1.97×10^{-5}	4.16×10^{-8}	1.07×10^{-8}	4.75×10^{-5}	2.72×10^{-7}
^{30}P	2.499 m	1.89×10^{-5}	9.85×10^{-9}	1.89×10^{-9}	4.30×10^{-5}	6.56×10^{-8}
^{32}P	14.29 d	1.70×10^{-4}	3.92×10^{-7}	1.02×10^{-7}	4.13×10^{-4}	2.50×10^{-6}
^{33}P	25.4 d	2.43×10^{-4}	9.21×10^{-7}	2.35×10^{-7}	6.18×10^{-4}	$6.13 \times 10^{-}$
^{35}P	47.4 s	1.65×10^{-5}	1.00×10^{-7}	2.47×10^{-8}	4.44×10^{-5}	7.06×10^{-7}
^{35}S	87.44 d	1.81×10^{-4}	1.37×10^{-6}	3.41×10^{-7}	4.98×10^{-4}	9.71×10^{-6}
^{37}S	5.06 m	4.03×10^{-5}	4.48×10^{-7}	8.98×10^{-8}	1.18×10^{-4}	3.44×10^{-6}
^{38}S	2.87 h	3.08×10^{-5}	2.67×10^{-7}	7.12×10^{-8}	8.70×10^{-5}	1.81×10^{-6}
^{34m}Cl	32.0 m	7.76×10^{-6}	2.42×10^{-8}	7.19×10^{-9}	1.97×10^{-5}	1.50×10^{-7}
^{36}Cl	3.01×10^{5} y	4.00×10^{-4}	3.81×10^{-6}	1.01×10^{-6}	1.16×10^{-3}	2.76×10^{-5}
^{38}Cl	37.21 m	2.85×10^{-4}	3.39×10^{-6}	7.88×10^{-7}	8.41×10^{-4}	2.55×10^{-5}
^{39}Cl	55.6 m	5.21×10^{-4}	5.27×10^{-6}	1.21×10^{-6}	1.48×10^{-3}	3.96×10^{-5}
^{40}Cl	1.4 m	5.46×10^{-5}	1.04×10^{-6}	1.97×10^{-7}	1.75×10^{-4}	8.44×10^{-6}
^{37}Ar	35.02 d	4.64×10^{-4}	2.68×10^{-5}	2.48×10^{-6}	1.25×10^{-3}	5.12×10^{-5}
^{39}Ar	269.0 y	1.57×10^{-3}	2.03×10^{-5}	2.91×10^{-6}	4.57×10^{-3}	1.70×10^{-4}
^{41}Ar	1.827 h	7.72×10^{-3}	9.23×10^{-4}	7.10×10^{-5}	1.69×10^{-2}	1.03×10^{-3}
^{38}K	7.636 m	4.86×10^{-6}	7.24×10^{-9}	1.26×10^{-9}	1.34×10^{-5}	7.14×10^{-8}
^{40}K	1.28×10^{9} y	1.90×10^{-5}	6.40×10^{-8}	1.20×10^{-8}	5.67×10^{-5}	6.03×10^{-7}

6. Determination of the release

In an experimental cavern of the LHC, the change in the number of nuclei, N, of a given radionuclide per unit time is the difference between the production rate and the sum of the decay and extraction rates. P is defined as the number produced per p-p collision of the radionuclide whose mean life-time is τ (the decay constant $\lambda = 1/\tau$). The volume of fresh air cycled through the area per second is Q and the volume of air in the area V_{irr}. It is also assumed that there is complete mixing of the air inside the cavern, so that a radionuclide has the same probability of being removed from the cavern no matter where it is produced. Thus:

$$\frac{\mathrm{d}N}{\mathrm{d}t} = P\nu_c(t) - \left(\frac{N}{\tau} + \frac{Q}{V_{irr}}N\right) = P\nu_c(t) - (\lambda + m)N, \tag{1}$$

where Q/V_{irr} is defined as the air-extraction rate from the cavern, m and ν_c is the inelastic p-p collision rate, which can vary with time. During the i'th fill, starting at $t = 0$, equation (1) has the solution

$$N = \exp[-(\lambda + m)t]\left(N_i + P\int_0^t \nu_c(t)\exp[(\lambda + m)t]\mathrm{d}t\right), \tag{2}$$

where N_i nuclei remain from previous fills.

The inelastic p-p collision rate $\nu_c(t)$ is the product of the luminosity, $\mathcal{L}(t)$, and the inelastic cross-section, σ_{inel}, and is given by:

$$\nu_c(t) = \mathcal{L}(t)\sigma_{\mathrm{inel}} = \mathcal{N}(t)^2\frac{\mathcal{L}_0}{\mathcal{N}_0^2}\sigma_{\mathrm{inel}}, \tag{3}$$

where $\mathcal{N}(t)$ is the number of protons in one circulating beam at the time t and $\mathcal{N}_0$ and $\mathcal{L}_0$ are the values at the start of the fill.

$\mathcal{N}(t)$ is the solution of the equation:

$$\frac{\mathrm{d}\mathcal{N}}{\mathrm{d}t} = -\frac{1}{\mathcal{N}_0\tau_b}\mathcal{N}^2 - \frac{1}{\tau_g}\mathcal{N}, \tag{4}$$

where the initial half-life of the beam due to beam-beam collisions τ_b is equal to $\mathcal{N}_0/(\sigma_{tot}\mathcal{L}_0 n_x)$. The total cross-section for p-p interactions is σ_{tot} and n_x is the number of experimental areas operating simultaneously. τ_g is the lifetime of the beam due to beam-gas interactions.

The solution of Equation (4) is:

$$\mathcal{N} = \frac{\mathcal{N}_0\exp[-t/\tau_g]}{(\tau_g/\tau_b)(1 - \exp[-t/\tau_g]) + 1}, \tag{5}$$

and this can be substituted into Equation (3) to give $\nu_c(t)$.

The activity of the radionuclide extracted from the experimental cavern is $m\lambda N$, where N is given by equation (2) Thus the rate of release in Bq per second of the radionuclide into the atmosphere is:

$$R = m\lambda N\exp[-\lambda t_d], \tag{6}$$

where t_d is the decay time during which the activated air passes through the ventilation ducts from the experimental area before it reaches the outside world.

The total activity vented to the atmosphere during the i'th fill, which lasts for a time t_{fill}, is obtained by integrating the above equation:

$$Y_i^{(on)} = \int_0^{t_{fill}} R \, dt. \tag{7}$$

At the end of the fill, the number of radionuclei in the experimental area, N_i', is given by substituting t_{fill} into equation (2). If the time between fills is t_{off}, the number remaining at the start of the next fill is:

$$N_{i+1} = N_i' \exp[-(\lambda + m_{off})t_{off}]. \tag{8}$$

where the air-extraction rate during the down-time between fills, m_{off}, could well be different from the value of m during a fill because of a different ventilation rate Q_{off}.

The total activity vented after the i'th fill during the time between fills is:

$$\begin{aligned} Y_i^{(off)} &= m\lambda \exp(-\lambda t_d^{off}) \int_0^{t_{off}} N_i' \exp[-(\lambda + m_{off})t] dt, \\ &= \frac{m\lambda}{m+\lambda} \exp(-\lambda t_d^{off}) N_i' \, (1 - \exp[-(\lambda + m_{off})t_{off}]). \end{aligned} \tag{9}$$

In the calculation of the total release during one year of operation the contributions from successive fills are summed:

$$Y_{tot} = \sum_i (Y_i^{(on)} + Y_i^{(off)}), \tag{10}$$

remembering that after the final fill the integration in equation (9) has to be taken to infinity rather than to t_{off}.

It was suggested by Höfert *et al.* [Hof95] that the environmental significance of releases of radioactivity from the LHC should be based on the maximum beam intensities which could be obtained: a maximum number of protons in one ring of 4.7×10^{14} protons at 7 TeV and an ultimate luminosity of $2.5 \times 10^{34}\,cm^{-2}s^{-1}$. On the assumption of one fill of 20 hours duration every 24 hours and a beam-gas lifetime of 250 hours, the average collision rate in either of the two high-luminosity experiments would be $7.5 \times 10^8\,s^{-1}$, calculated using Equation (3) [Pot95]. The inelastic and elastic p-p cross-sections were taken to be 70 and 40 mbarns respectively. However Höfert *et al.* suggested that an average collision rate of $10^9\,s^{-1}$ should be taken. Thus in order to obtain the time variation of the collision rate in an experiment, values determined using Equation (1) have been scaled by the factor of $10^9/7.5 \times 10^8 = 1.33$.

For determining the annual release of radioactivity from the experimental cavern, the number of days of operation of the LHC in a year was taken as 180, [Hof95]. The air exchange rate was 2 per hour and 95% of the air was assumed to be recycled. This led to a value for the air extraction rate, m, of $0.1\,h^{-1}$. The delay between the time the air leaves the cavern and the time the air is released is 15 seconds [Hat95]. However it is assumed that the shafts (which are completely closed during operation) will be ventilated with fresh air at the end of each 60 day operating period.

The calculated annual release of radioactivity from the ATLAS and CMS caverns is given in columns 2 and 3 of Table 4. Despite the accumulation of radionuclides, to within a few percent, the release during a single fill is one-180'th of these values.

These releases from the caverns are compared with the present CERN Design Constraints in Table 5 where it will be seen that even for the short-lived β/γ radionuclides from the CMS cavern,

Table 4: Release of Radioactivity in the Air from the Experimental Regions

Radionuclide	Experimental Caverns Annual release (Bq)		Shafts Release per period (Bq)		
	ATLAS	CMS	ATLAS–Big	ATLAS–Small	CMS
^{3}H	1.39×10^{6}	3.07×10^{6}	1.86×10^{3}	3.77×10^{2}	1.46×10^{4}
^{7}Be	3.48×10^{7}	8.25×10^{7}	2.17×10^{4}	5.29×10^{3}	1.60×10^{5}
^{10}Be	1.82×10^{0}	5.54×10^{0}	8.69×10^{-3}	1.70×10^{-3}	6.99×10^{-2}
^{11}C	9.76×10^{9}	2.63×10^{10}	5.29×10^{4}	1.23×10^{4}	4.03×10^{5}
^{14}C	2.18×10^{5}	4.67×10^{5}	8.24×10^{3}	6.35×10^{2}	9.35×10^{3}
^{13}N	9.87×10^{8}	2.85×10^{10}	1.36×10^{5}	2.86×10^{4}	1.05×10^{6}
^{14}O	4.68×10^{8}	1.38×10^{9}	2.65×10^{3}	6.17×10^{2}	2.15×10^{4}
^{15}O	6.39×10^{9}	1.85×10^{10}	6.05×10^{4}	1.39×10^{4}	4.46×10^{5}
^{19}O	8.56×10^{5}	1.63×10^{6}	1.27×10^{-1}	1.93×10^{-2}	1.03×10^{0}
^{18}F	1.68×10^{7}	3.41×10^{7}	1.27×10^{1}	1.57×10^{0}	9.22×10^{1}
^{23}Ne	1.82×10^{6}	3.60×10^{6}	8.15×10^{-1}	1.30×10^{-1}	5.79×10^{0}
^{24}Ne	5.97×10^{5}	1.15×10^{6}	9.59×10^{-2}	1.49×10^{-2}	7.29×10^{-1}
^{22}Na	2.32×10^{3}	4.82×10^{3}	5.63×10^{-1}	1.03×10^{-1}	3.45×10^{0}
^{24}Na	3.12×10^{6}	6.71×10^{6}	2.17×10^{1}	4.61×10^{0}	1.37×10^{2}
^{25}Na	3.62×10^{6}	7.34×10^{6}	2.42×10^{0}	4.02×10^{-1}	1.62×10^{1}
^{27}Mg	4.18×10^{6}	9.16×10^{6}	6.08×10^{0}	1.08×10^{0}	3.90×10^{1}
^{28}Mg	3.82×10^{5}	8.94×10^{5}	7.60×10^{0}	1.64×10^{0}	4.77×10^{1}
^{26}Al	1.23×10^{-2}	2.59×10^{-2}	2.21×10^{-6}	3.88×10^{-7}	1.45×10^{-5}
^{28}Al	2.47×10^{7}	5.54×10^{7}	3.98×10^{1}	7.77×10^{0}	2.50×10^{2}
^{29}Al	7.90×10^{6}	1.84×10^{7}	1.93×10^{1}	3.76×10^{0}	1.20×10^{2}
^{31}Si	1.14×10^{7}	2.66×10^{7}	4.01×10^{1}	9.47×10^{0}	2.57×10^{2}
^{32}Si	1.50×10^{1}	3.61×10^{1}	1.05×10^{-2}	2.72×10^{-3}	6.90×10^{-2}
^{30}P	7.61×10^{6}	1.74×10^{7}	6.00×10^{0}	1.15×10^{0}	4.00×10^{1}
^{32}P	1.45×10^{6}	3.54×10^{6}	3.70×10^{2}	9.64×10^{1}	2.36×10^{3}
^{33}P	1.18×10^{6}	3.00×10^{6}	7.42×10^{2}	1.90×10^{2}	4.94×10^{3}
^{35}P	5.72×10^{6}	1.54×10^{7}	6.08×10^{1}	1.50×10^{1}	4.29×10^{2}
^{35}S	2.58×10^{5}	7.09×10^{5}	5.19×10^{2}	1.29×10^{2}	3.68×10^{3}
^{37}S	1.68×10^{7}	4.91×10^{7}	2.74×10^{2}	5.49×10^{1}	2.10×10^{3}
^{38}S	9.40×10^{6}	2.66×10^{7}	2.07×10^{2}	5.53×10^{1}	1.41×10^{3}
^{34m}Cl	3.12×10^{6}	7.92×10^{6}	1.53×10^{1}	4.55×10^{0}	9.47×10^{1}
^{36}Cl	4.55×10^{-1}	1.31×10^{0}	1.45×10^{-3}	3.81×10^{-4}	1.04×10^{-2}
^{38}Cl	1.13×10^{8}	3.40×10^{8}	2.16×10^{3}	5.02×10^{2}	1.62×10^{4}
^{39}Cl	1.98×10^{8}	5.63×10^{8}	3.44×10^{3}	7.90×10^{2}	2.58×10^{4}
^{40}Cl	2.09×10^{7}	6.70×10^{7}	6.31×10^{2}	1.20×10^{2}	5.14×10^{3}
^{37}Ar	1.64×10^{6}	4.41×10^{6}	1.86×10^{4}	1.72×10^{3}	3.56×10^{4}
^{39}Ar	2.00×10^{3}	5.81×10^{3}	8.61×10^{0}	1.23×10^{0}	7.21×10^{1}
^{41}Ar	2.64×10^{9}	5.76×10^{9}	6.54×10^{5}	5.03×10^{4}	7.30×10^{5}
^{38}K	2.05×10^{6}	5.63×10^{6}	4.44×10^{0}	7.71×10^{-1}	4.37×10^{1}
^{40}K	5.09×10^{-6}	1.51×10^{-5}	5.70×10^{-9}	1.07×10^{-9}	5.37×10^{-8}

where the release is higher than for ATLAS, the annual release is never more than one per mil of the Design Constraint. The results from the 1992 study [Ste92] are also given in Table 5 for comparison. Most of the new values are almost an order of magnitude lower than the previous study, mainly due to the fact that there is now significant shielding around the forward detector, collimator and low-beta quadrupoles. However, since more radionuclides are considered in the present study, the release of the long-lived radionuclides is approximately the same as before.

The releases from the shafts were determined on the basis of closed ventilation systems for a 60 day operating period and the extraction of the air immediately after the last fill of the period. The variation in production rate during a fill was taken into account as for the caverns. The results of the calculations are given in the last three columns of Table 4 and the annual releases are summarized in Table 6. It will be seen that the release values are insignificant when compared to the CERN Design Constraints.

Table 5: Annual release of radioactivity in the air from the Experimental Caverns (Bq)

Nuclide	CERN Constraint (Bq)	1992 Studies Partial (Bq)	ATLAS (Bq)	CMS (Bq)
^{3}H	4×10^{12}	2.0×10^{7}	1.39×10^{6}	3.07×10^{6}
^{7}Be	4×10^{11}	4.3×10^{8}	3.48×10^{7}	8.25×10^{7}
All β/γ with $T_{1/2} < 1$ d	1.2×10^{14}	4.7×10^{11}	2.96×10^{10}	8.16×10^{10}
Other β/γ with $T_{1/2} > 1$ d	4×10^{10}	5.9×10^{6}	4.75×10^{6}	1.21×10^{7}

Table 6: Annual release of radioactivity in the air from the Experimental Shafts (Bq)

Nuclide	CERN Limit Bq	ATLAS Big Shaft	ATLAS Small Shaft	CMS
^{3}H	4×10^{12}	5.57×10^{3}	1.13×10^{3}	4.37×10^{4}
^{7}Be	4×10^{11}	6.50×10^{4}	1.59×10^{4}	4.81×10^{5}
All β/γ with $T_{1/2} < 1$ d	1.2×10^{14}	2.74×10^{6}	3.22×10^{5}	8.10×10^{6}
Other β/γ with $T_{1/2} > 1$ d	4×10^{10}	8.55×10^{4}	8.32×10^{3}	1.68×10^{5}

7. Off-site doses and dose rates

Two release scenarios are considered here. The first is a continuous long-term release which is assumed to take place at a constant rate. The dose is calculated for the year of interest after 50 years of continuous operation at the same level of emission. The history of previous emissions is important for the long-lived radioactive species which may accumulate in the environment and for which the radioactive emissions over the entire life-time of the facility must be considered. For this long-term emission scenario, the dispersion in the atmosphere was determined by averaging over meteorological conditions such as wind speed and direction. In the long-term scenario the annual dose (in the case of ingestion and inhalation this is the committed dose) is calculated for the current year. One takes into account however any radioactivity which may have been deposited up to that year from the previous 50 years of operation.

Such an averaging over long time scales could allow for a dilution of short term releases, which might exceed daily or weekly limits. Therefore a second scenario was considered, where a short term release is assumed to take place over a period of approximately 24 hours during which the meteorological conditions are assumed to be constant and such that they lead to the highest probable off-site dose. The source term is provided by one fill cycle starting at some instant of time, t=0. In this scenario the total dose from a single release is calculated, including an integration to t=50 years in order to account for the radioactivity deposited in the environment. The time-scale for the two scenarios is illustrated in Figure 4.

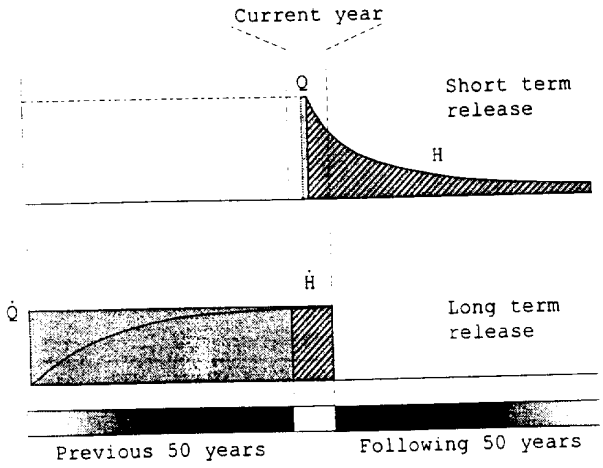

Figure 4: Time scale for short and long term release calculations. Note that the 'current year' in the upper plot can be any year during operation, while it is 50 years after machine start-up in the lower plot.

A height-corrected Gaussian plume model as recommended by IAEA Safety Guide 50-SG-S3 was used to calculate the atmospheric dispersion. The dispersion parameters used were those parametrized by Briggs [Bri74] and include a correction for terrain roughness. This roughness correction is based on the fact that when the radioactive plume extends downwind it remains narrow in a smooth landscape which introduces little dispersion. The turbulence introduced by buildings and other surface roughnesses spreads out the plume more quickly. These effects are parametrized by roughness lengths, which are given in Table 7.

Table 7: Roughness lengths of different landscape types

Length	Landscape type
1 cm	Lawn grass, bodies of water
4 cm	Ploughed land
10 cm	Open grass land
40 cm	Rural areas with mixed farming, woods
100 cm	Cities and forests
400 cm	Cities with tall buildings

The exhaust for the CMS experimental cavern will be located in a region of open countryside and therefore a terrain roughness-length of 10 cm was assumed for this site. The ATLAS experiment however will be located underneath an area which is more built-up with light industrial construction. A terrain roughness length of 100 cm was therefore chosen for this site.

The external dose due to gamma rays was calculated by integrating the contribution from a

given volume element over the entire plume. For short distances from the emission point this gives a better estimate than the simpler, semi-infinite cloud approximation.

The values for the exhaust parameters for both ATLAS and CMS were [Hat95]:

Stack height (h)	=	20 m
Stack diameter (d)	=	100 cm
Exhaust speed (W_0)	=	10 m s^{-1}

The atmospheric dispersion may be characterized by the ground level, centre-line dispersion factors which represent the atmospheric radioactivity concentration at ground level on the axis of the plume normalized to unit release of radioactivity. The dispersion factors for the different atmospheric stability classes (Pasquill categories [Pas61]) are shown in Figure 5 as a function of distance from the CMS release point. For the short-term release, the dispersion factor for atmospheric stability class B (sunny and warm with a wind speed less than 5 m s^{-1}) was selected as this has the highest value over the largest range of distances. Also shown in Figure 5 is the long-term dispersion factor in the most likely wind direction weighted for the atmospheric stability class distribution for the year and for the frequency of the wind blowing in that direction.

The dispersion factors for the ATLAS experiment are shown in Figure 6. Because of the greater terrain roughness chosen for this site the dispersion is greater and the pronounced fall-off in concentration for short distances is not seen. It must be remembered that these dispersion factors do not take into account the decay during flight as this is radionuclide specific.

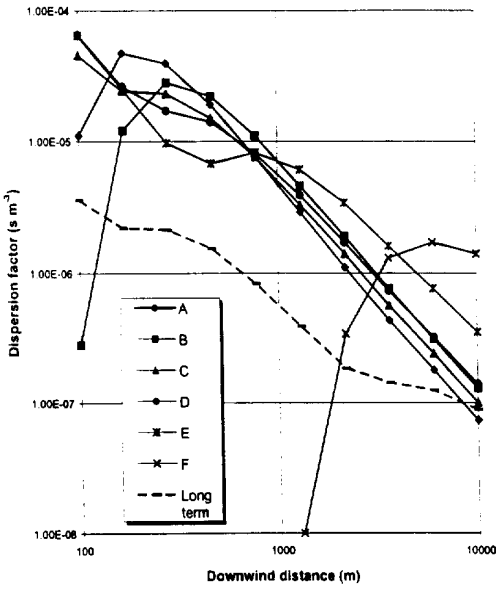

Figure 5: Atmospheric dispersion factors for releases from the CMS cavern, Pasquill categories A–F (terrain roughness length $z_0 = 10$ cm)

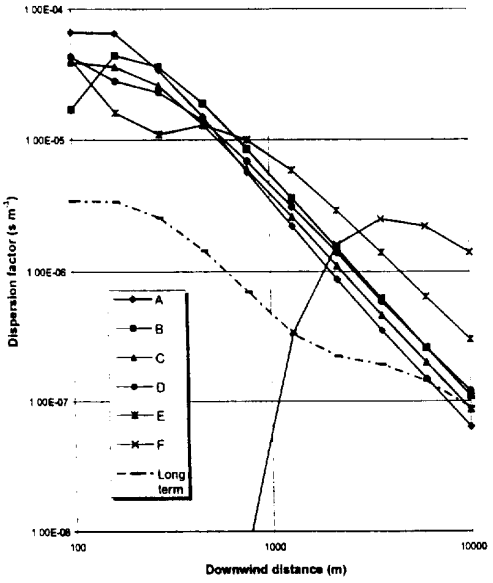

Figure 6: Atmospheric dispersion factors for releases from the ATLAS cavern, Pasquill categories A–F (terrain roughness length $z_0 = 100$ cm)

In this report the dose has been examined as a function of distance from the release points rather than defining a specific critical group of persons who live at a particular location relative to the release point. Figure 7 shows the dose from a short term release from CMS (*i.e.* one fill cycle of the accelerator) as a function of distance for the seven radionuclides which are the major contributors. These are the radionuclides traditionally considered important, except perhaps for ^{32}P. Data exist

for all radionuclides, but for clarity they have been omitted from Figure 7. The rapid fall-off with distance for the short-lived species is a direct consequence of their decay during flight; the shorter the half-life the more rapidly the dose declines with distance. The largest contribution to the dose from ^{32}P is the ingestion dose. Figure 8 presents the annual dose for the long term release for the same radionuclides from CMS. It will be seen that the different radionuclides maintain their relative importances.

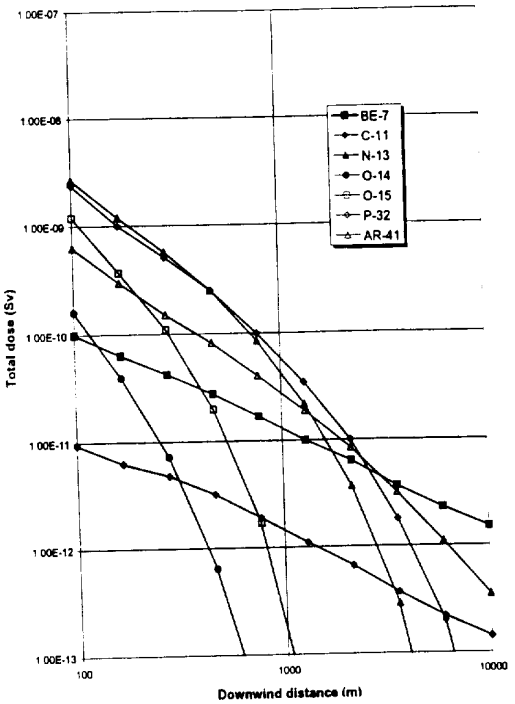

Figure 7: The dose due to radioactive releases for the seven dominant radionuclides from one fill cycle, CMS experimental area

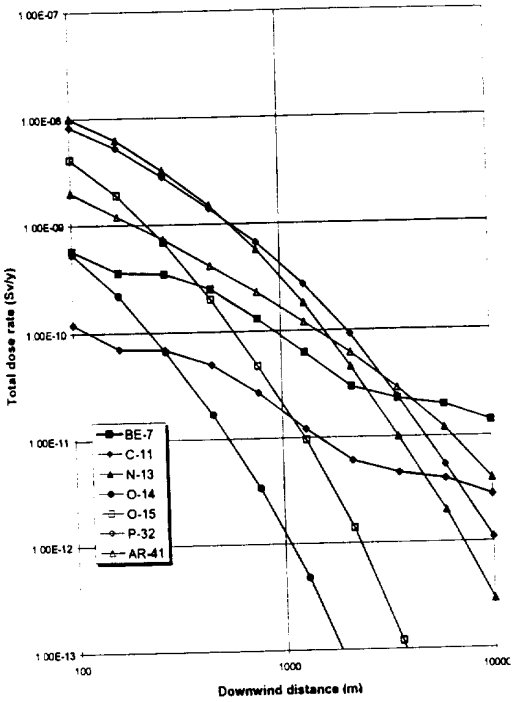

Figure 8: The annual dose rate due to radioactive releases for the seven dominant radionuclides, CMS experimental area

The relative importance of the exposure from external sources, such as cloud activity and ground deposition, and inhalation and ingestion is investigated in Figures 9 and 10. As far as ingestion is concerned, it is unreasonable to expect that any persons exposed at a given distance from the release point will be able to cover all their food intake from plants and animals raised at that same location. This is made even more unlikely because of the wide availability of imported fruit and vegetables from outside the affected regions and the homogenization of the food industry within the European community. In the present calculations, an overall fraction of 10% was applied to the intake of all food from the local area. With this assumption it can be seen in Figures 9 and 10 that the activity deposited on the ground becomes important relative to the other contributors at distances greater than several kilometres from the release point. This is in part due to the fact that the major contributors to the external dose are short-lived and so have decayed before they are transported to large distances by the wind.

The total dose due to a single fill and the long term dose rate for all radionuclides considered are presented as a function of distance in Figure 11. To test the sensitivity of the calculation to the fraction of food taken from the local area, the total dose was also calculated assuming 100% food intake from the local area. In Figure 11 the total dose and dose rate are shown with both 10% and 100% of the food intake coming from the local area. As expected at larger distances the percentage uptake of food from the affected point plays a major role, but it will be seen that in absolute terms,

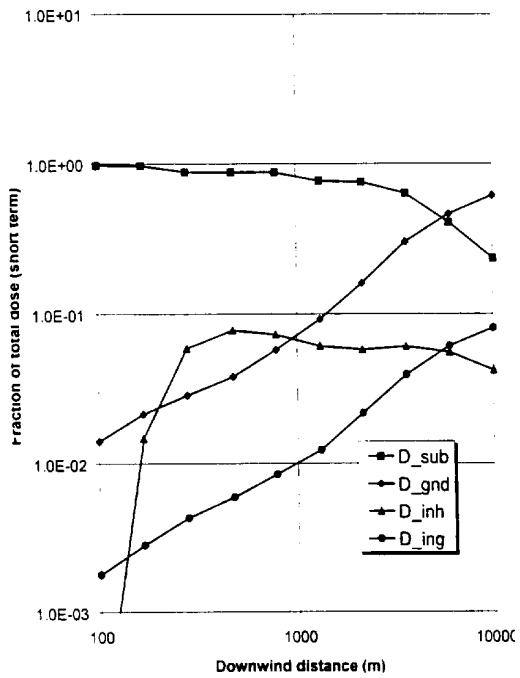

Figure 9: The fraction of the dose from different sources for a release over one fill cycle, CMS experimental area. ■ – external exposure from cloud activity, ♦ – external exposure from ground activity, ▲ – internal exposure from inhalation and • – internal exposure from ingestion.

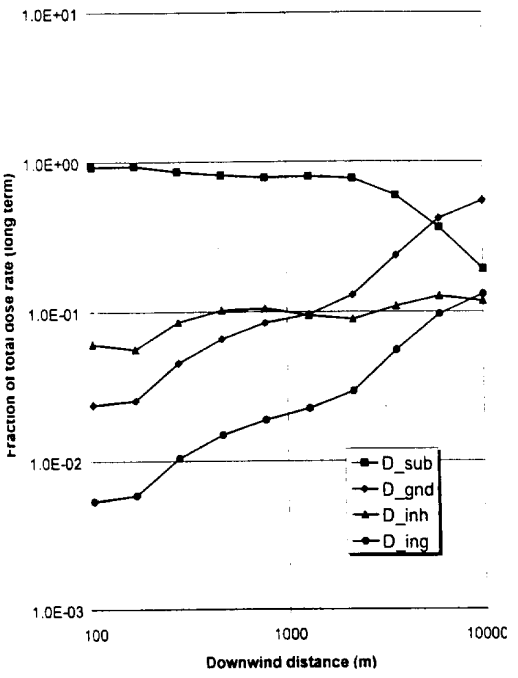

Figure 10: The fraction of the dose from different sources for a release over one year, CMS experimental area. ■ – external exposure from cloud activity, ♦ – external exposure from ground activity, ▲ – internal exposure from inhalation and • – internal exposure from ingestion.

the dose is three orders of magnitude lower at these large distances than at 100 metres. The distribution of dose with distance is very similar for the ATLAS experimental area (see Figure 12) and so only the total dose for the short term (one fill) and the annual dose for the long term releases are presented (for a 10% food intake).

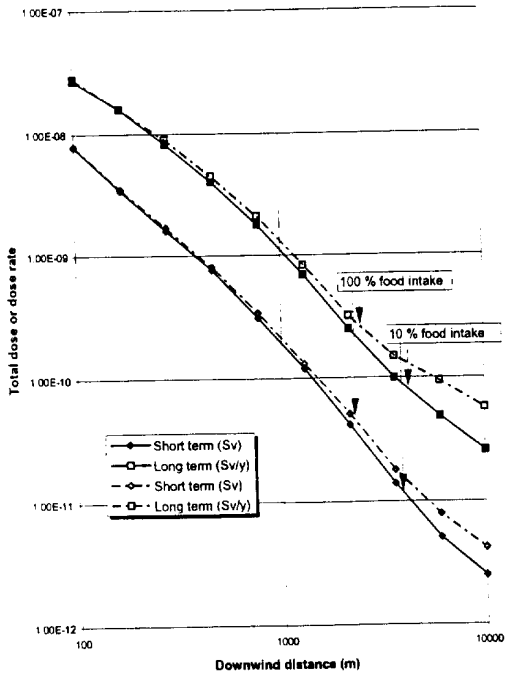

Figure 11: Dose as a function of distance for single-fill and annual releases from the CMS experimental area.

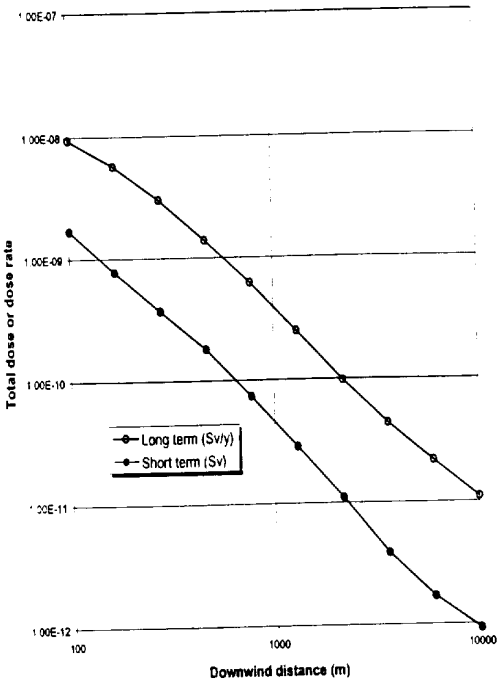

Figure 12: Dose as a function of distance for single-fill and annual releases from the ATLAS experimental area.

From these Figures it can be seen that for distances greater than 100 m (in the most frequent wind direction) the average annual dose never exceeds $\approx 0.05\ \mu$Sv per year for the CMS experimental area and $\approx 0.01\ \mu$Sv per year for the ATLAS experimental area. For the releases from a single fill cycle which assume an atmospheric stability category which yields the highest possible concentration of radioactivity, the dose at distances greater than 100 m does not exceed $\approx 0.01\ \mu$Sv for the CMS experimental area and $\approx 0.002\ \mu$Sv for the ATLAS experimental area.

The doses from releases from the shafts after a 60-day period of operation are shown in Figure 13, calculated for a ground-level release with no vertical velocity given to the exhaust, but with the same atmospheric short-term release assumptions as before. It will be seen that the doses are almost two orders of magnitude lower than the short-term releases from the caverns.

8. Conclusions

The present calcuations of the production and release of radionuclides in the ventilations systems of the two high-luminosity experiments ATLAS and CMS have shown that the activities released in one year are less than one per mil of the current CERN Design constraints.

The maximum annual dose from these releases has been estimated and shown that it never exceeds the equivalent of 25 minutes of exposure to natural background radiation.

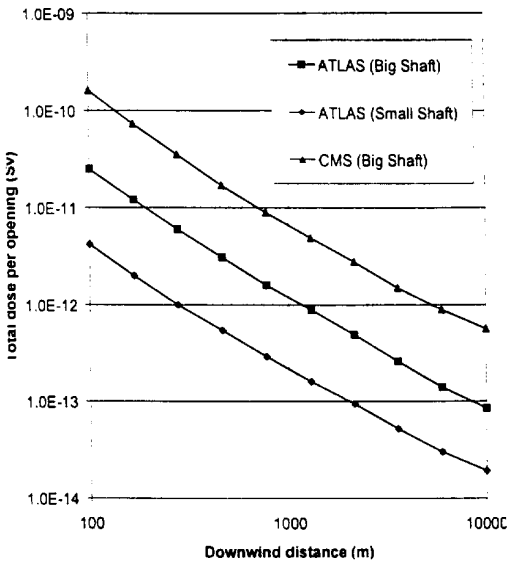

Figure 13: Dose as a function of distance for releases from the shafts of the ATLAS and CMS experimental areas.

References

[Aur94] P. Aurenche, F. Bopp, R. Engel, D. Pertermann, J. Ranft and S. Roesler, *DTUJET–93, Sampling inelastic proton-proton and proton-antiproton collisions according to the two-component dual parton model*, Comput. Phys. Commun. 83 (1994) 107.

[Bri74] G. A. Briggs, *Diffusion Estimates for Small Emissions*, Environmental Research Laboratories, Air Resources, Atmosphere, Turbulence and Diffusiion Laboratory, Annual Report 1973 US-AFC Report ATDL-106, National Oceanic and Atmospheric Administration (1974).

[Fas93] A. Fassò, A. Ferrari, J. Ranft and P. R. Sala, *FLUKA: present status and future developments*, Proc IV Int. Conf. on Calorimetry in High Energy Physics, La Biodola (Isola d'Elba), Sept. 20–25 1993. Ed. A. Menzione and A. Scribano, World Scientific, p. 493 (1993).

[Fas94] A. Fassò, A. Ferrari, J. Ranft and P. R. Sala, *FLUKA: Performances and Applications in the Intermediate Energy Range*, Specialists' Meeting on Shielding Aspects of Accelerators, Targets and Irradiation Facilities. Arlington, Texas, April 28–29 1994, NEA/OECD (Paris) p. 287.

[Fer96] A. Ferrari, K. Potter, S. Rollet and P. R. Sala, *Radiation calculations for the ATLAS detector and experimental hall*, presented at the 2nd Workshop on Simulating Accelerator Radiation Environments, 9–11th October 1995, CERN.

[Hat95] M. Hatch, private communication (1995).

[Hof95] M. Höfert, K. Potter and G. R. Stevenson, *Summary of Design Values, Dose Limits, Interaction Rates etc. for use in estimating Radiological Quantities associated with LHC Operation*, CERN Internal Report TIS–RP/IR/95–19 (1995).

[HSK95] Hauptabteilung für die Sicherheit der Kernanlagen (HSK), *Berechnung der Strahlenexposition in der Umgebung aufgrund von Emissionen radioaktiver Stoffe aus Kernanlagen*, HSK-R-41/d (April 1995).

[Huh95a] M. Huhtinen, *Radiation environment simulations for the CMS detector*, presented at the 2nd Workshop on Simulating Accelerator Radiation Environments, 9–11th October 1995, CERN.

[Huh95b] M. Huhtinen and G. R. Stevenson, *Shielding requirements in the CMS experimental region*, CERN Internal Report CERN/TIS–RP/IR/95–15 (1995): CERN CMS/TN 95–056.

[Huh95c] M. Huhtinen and G. R. Stevenson, *Energy deposition, star densities and shielding requirements around the inner triplet of the high-luminosity insertions of the LHC*, CERN Divisional Report CERN/TIS–RP/95-11 (1995): LHC Note 338.

[IAEA80] International Atomic Energy Agency, *Atmospheric Dispersion in Nuclear Power Plant Siting*, IAEA Safety Guide No.50-SG-S3, (1980).

[ICRP83] ICRP Publication 38, *Radionuclide transformations, energy and intensity of emissions*, International Commission on Radiological Protection, Pergamon Press [Oxford and New York] (1983).

[Ilj93] A. S Iljinov,V. G. Semenov, M. P. Semenova, N. M. Sobolevskym and L. V. Udovenko, *Production of Radionuclides at Intermediate Energies*, Landolt-Börnstein, Numerical data and Functional Relationships in Science and Technology, New Series, Group I: Nuclear and Particle Physics, Volume 13a–e, ed. H.Schopper, Springer-Verlag [Berlin] (1991–1993).

[Mor96] L. E. Moritz, *Implementation of the Draft Swiss Standard HSK-R-41/d to calculate Off-site Doses and Dose Rates due to Radioactive Emissions from CERN*, to be published.

[Pas61] F. Pasquill, *The estimation of the dispersion of windborne material*, Met. Mag. 90 (1961) 33.

[Pot95] K. Potter and G. R. Stevenson, *Average interaction rates for shielding specification in High-Luminosity LHC Experiments*, CERN Internal Report TIS–RP/IR/95–05 (1995), CERN AC/95–01, LHC Note 310.

[Sil90] R. Silberberg and C. H. Tsao, *Spallation processes and nuclear interaction products of cosmic rays*, Physics Reports 191 (1990) 351–408.

[Ste92] G. R. Stevenson, A. Fassò, J-P. Munich and J. M. Zazula, *The estimation of parameters of radiological interest in and around an LHC experimental area*, CERN Internal Report TIS–RP/IR/92–06 (1992).

APPENDIX-A

Nuclei produced per p-p event in the regions of ATLAS

Region	1	2	3	4	5	6	7
Radionuclide							
H-3	1.50E-02	3.45E-04	1.71E-03	3.17E-02	1.26E-03	2.02E-04	4.11E-05
Be-7	5.24E-03	1.01E-04	4.88E-04	8.84E-03	2.87E-04	4.00E-05	9.77E-06
Be-10	1.87E-03	1.47E-04	2.28E-04	5.57E-03	7.07E-04	1.22E-04	2.38E-05
C-11	8.21E-03	2.15E-04	7.62E-04	1.37E-02	6.17E-04	8.49E-05	1.98E-05
C-14	1.64E+00	2.15E-01	2.16E-02	6.31E-01	1.14E+00	4.14E-01	3.19E-02
N-13	5.98E-03	2.98E-04	7.05E-04	1.50E-02	1.37E-03	2.21E-04	4.65E-05
O-14	4.44E-04	1.33E-05	4.10E-05	7.22E-04	3.33E-05	4.36E-06	1.02E-06
O-15	5.28E-03	1.87E-04	4.91E-04	9.48E-03	6.51E-04	9.94E-05	2.28E-05
O-19	9.38E-07	6.86E-09	1.08E-07	1.85E-06	2.65E-09	2.08E-10	3.17E-11
F-18	1.59E-05	1.64E-07	1.81E-06	3.10E-05	1.51E-07	1.79E-08	2.21E-09
Ne-23	1.98E-06	1.78E-08	2.26E-07	3.88E-06	1.29E-08	1.34E-09	2.13E-10
Ne-24	4.70E-07	3.67E-09	5.38E-08	9.25E-07	1.75E-09	1.57E-10	2.45E-11
Na-22	5.79E-06	6.90E-08	6.39E-07	1.10E-05	9.13E-08	1.31E-08	2.40E-09
Na-24	7.43E-06	1.01E-07	8.28E-07	1.43E-05	1.59E-07	2.23E-08	4.72E-09
Na-25	3.22E-06	3.33E-08	3.67E-07	6.32E-06	3.37E-08	3.97E-09	6.62E-10
Mg-27	3.14E-06	4.35E-08	3.58E-07	6.26E-06	7.92E-08	9.91E-09	1.76E-09
Mg-28	1.12E-06	2.08E-08	1.26E-07	2.23E-06	5.31E-08	7.71E-09	1.66E-09
Al-26	8.69E-06	1.09E-07	9.21E-07	1.58E-05	1.15E-07	1.39E-08	2.43E-09
Al-28	2.18E-05	3.33E-07	2.13E-06	3.69E-05	5.10E-07	6.54E-08	1.28E-08
Al-29	6.18E-06	1.05E-07	6.57E-07	1.16E-05	2.38E-07	3.15E-08	6.14E-09
Si-31	1.38E-05	2.36E-07	1.18E-06	2.06E-05	4.56E-07	5.27E-08	1.24E-08
Si-32	7.49E-06	1.39E-07	6.25E-07	1.11E-05	3.35E-07	4.16E-08	1.07E-08
P-30	7.25E-06	1.12E-07	6.28E-07	1.08E-05	1.24E-07	9.85E-09	1.89E-09
P-32	6.50E-05	1.22E-06	5.32E-06	9.49E-05	3.17E-06	3.92E-07	1.02E-07
P-33	9.00E-05	1.99E-06	7.42E-06	1.37E-04	6.75E-06	9.21E-07	2.35E-07
P-35	5.68E-06	1.62E-07	4.82E-07	9.48E-06	6.77E-07	1.00E-07	2.47E-08
S-35	5.88E-05	1.93E-06	5.19E-06	1.06E-04	8.94E-06	1.37E-06	3.41E-07
S-37	9.64E-06	6.75E-07	1.20E-06	2.61E-05	2.71E-06	4.48E-07	8.98E-08
S-38	9.19E-06	3.37E-07	9.00E-07	1.86E-05	1.71E-06	2.67E-07	7.12E-08
Cl-34	2.95E-06	6.02E-08	2.40E-07	4.32E-06	1.86E-07	2.42E-08	7.19E-09
Cl-36	1.17E-04	4.95E-06	1.14E-05	2.42E-04	2.50E-05	3.81E-06	1.01E-06
Cl-38	7.22E-05	3.82E-06	7.76E-06	1.80E-04	2.11E-05	3.39E-06	7.88E-07
Cl-39	1.39E-04	6.42E-06	1.50E-05	3.29E-04	3.21E-05	5.27E-06	1.21E-06
Cl-40	7.56E-06	1.14E-06	1.36E-06	3.86E-05	5.93E-06	1.04E-06	1.97E-07
Ar-37	1.64E-04	1.59E-05	8.19E-06	1.91E-04	8.44E-05	2.68E-05	2.48E-06
Ar-39	3.19E-04	3.00E-05	4.57E-05	1.07E-03	1.12E-04	2.03E-05	2.91E-06
Ar-41	3.64E-03	4.73E-04	3.93E-05	1.04E-03	2.53E-03	9.23E-04	7.10E-05
K-38	1.71E-06	4.24E-08	1.70E-07	2.87E-06	7.29E-08	7.24E-09	1.26E-09
K-40	6.88E-06	1.97E-07	8.13E-07	1.07E-05	4.83E-07	6.40E-08	1.20E-08

Nuclei produced per p-p event in the regions of CMS

Region	1	2	3	4	5	6
Radionuclide						
H-3	1.77E-02	1.31E-03	4.50E-02	2.79E-02	1.88E-02	1.59E-03
Be-7	7.02E-03	3.35E-04	1.54E-02	8.54E-03	4.15E-03	2.96E-04
Be-10	3.40E-03	6.47E-04	6.54E-03	4.59E-03	1.07E-02	9.81E-04
C-11	1.35E-02	7.27E-04	2.61E-02	1.39E-02	9.20E-03	6.47E-04
C-14	3.42E+00	5.83E-02	1.80E+00	3.25E-01	2.22E+00	4.70E-01
N-13	1.04E-02	1.28E-03	2.13E-02	1.34E-02	2.10E-02	1.71E-03
O-14	8.72E-04	4.02E-05	1.50E-03	7.66E-04	5.16E-04	3.53E-05
O-15	9.37E-03	6.88E-04	1.72E-02	9.27E-03	1.00E-02	7.32E-04
O-19	8.30E-07	2.16E-08	2.84E-06	1.75E-06	8.21E-08	1.70E-09
F-18	1.61E-05	5.34E-07	4.97E-05	2.99E-05	3.54E-06	1.30E-07
Ne-23	1.89E-06	5.74E-08	6.09E-06	3.70E-06	3.33E-07	9.53E-09
Ne-24	4.26E-07	1.16E-08	1.43E-06	8.77E-07	5.04E-08	1.19E-09
Na-22	6.20E-06	2.22E-07	1.78E-05	1.05E-05	1.87E-06	8.06E-08
Na-24	8.43E-06	3.34E-07	2.34E-05	1.38E-05	3.16E-06	1.40E-07
Na-25	3.25E-06	1.10E-07	1.00E-05	6.03E-06	7.97E-07	2.67E-08
Mg-27	3.61E-06	1.58E-07	1.03E-05	6.02E-06	1.62E-06	6.34E-08
Mg-28	1.45E-06	7.68E-08	3.67E-06	2.13E-06	9.86E-07	4.84E-08
Al-26	9.84E-06	3.24E-07	2.64E-05	1.52E-05	2.45E-06	9.13E-08
Al-28	2.74E-05	1.01E-06	6.48E-05	3.59E-05	9.33E-06	4.11E-07
Al-29	7.90E-06	3.76E-07	1.98E-05	1.12E-05	4.39E-06	1.96E-07
Si-31	1.90E-05	6.87E-07	3.87E-05	2.02E-05	6.49E-06	3.38E-07
Si-32	1.05E-05	4.31E-07	2.10E-05	1.09E-05	4.73E-06	2.72E-07
P-30	9.81E-06	2.91E-07	2.04E-05	1.07E-05	1.83E-06	6.56E-08
P-32	9.17E-05	3.85E-06	1.80E-04	9.35E-05	4.38E-05	2.50E-06
P-33	1.31E-04	6.90E-06	2.53E-04	1.33E-04	9.44E-05	6.13E-06
P-35	8.59E-06	6.24E-07	1.64E-05	8.92E-06	9.85E-06	7.06E-07
S-35	9.10E-05	7.88E-06	1.73E-04	9.76E-05	1.29E-04	9.71E-06
S-37	1.81E-05	3.06E-06	3.32E-05	2.28E-05	4.05E-05	3.44E-06
S-38	1.45E-05	1.42E-06	2.88E-05	1.67E-05	2.56E-05	1.81E-06
Cl-34	4.31E-06	2.03E-07	8.35E-06	4.32E-06	2.50E-06	1.50E-07
Cl-36	1.95E-04	2.07E-05	3.67E-04	2.14E-04	3.58E-04	2.76E-05
Cl-38	1.19E-04	1.71E-05	2.39E-04	1.53E-04	3.13E-04	2.55E-05
Cl-39	2.18E-04	2.79E-05	4.59E-04	2.88E-04	4.87E-04	3.96E-05
Cl-40	1.69E-05	5.46E-06	3.34E-05	2.93E-05	9.04E-05	8.44E-06
Ar-37	3.22E-04	1.78E-05	3.35E-04	1.58E-04	4.16E-04	5.12E-05
Ar-39	6.28E-04	1.29E-04	1.20E-03	8.95E-04	1.72E-03	1.70E-04
Ar-41	7.58E-03	9.24E-05	3.88E-03	5.20E-04	4.77E-03	1.03E-03
K-38	3.19E-06	1.23E-07	5.93E-06	3.08E-06	1.04E-06	7.14E-08
K-40	1.36E-05	6.05E-07	2.30E-05	1.24E-05	7.12E-06	6.03E-07